Estimating Remaining Carbon Budgets Using Emulators of CMIP6 Models

Martin Rypdal (martin.rypdal@uit.no)
UiT The Arctic University of Norway https://orcid.org/0000-0003-0053-665X
Niklas Boers
Free University of Berlin and University of Exeter
Hege-Beate Fredriksen
UiT The Arctic University of Norway
Kai-Uwe Eiselt
UiT The Arctic University of Norway
Andreas Johansen
UiT The Arctic University of Norway
Andreas Martinsen
UiT The Arctic University of Norway
Endre Falck Mentzoni
UiT The Arctic University of Norway
Rune Graversen
UiT The Arctic University of Norway
Kristoffer Rypdal
UiT The Arctic University of Norway

Article

Keywords: Remaining carbon budget (RCB), emulators, CMIP6 models, CO2

Posted Date: January 12th, 2021

DOI: https://doi.org/10.21203/rs.3.rs-104000/v2

Estimating remaining carbon budgets using emulators of CMIP6 models

Martin Rypdal[1]*, Niklas Boers[2,3,4], Hege-Beate Fredriksen[5], Kai-Uwe Eiselt[5], Andreas Johansen[1], Andreas Martinsen[1], Endre Falck Mentzoni[1], Rune G. Graversen[5] & Kristoffer Rypdal[1]

[1]*Department of Mathematics and Statistics, UiT – The Arctic University of Norway, Norway*

[2]*Department of Mathematics and Computer Science, Free University of Berlin, Berlin, Germany*

[3]*Potsdam Institute for Climate Impact Research, Potsdam, Germany*

[4]*Department of Mathematics and Global Systems Institute, University of Exeter, Exeter, UK*

[5]*Department of Physics and Technology, UiT The Arctic University of Norway, Norway*

**Corresponding author address:* Martin Rypdal, UiT – The Arctic University of Norway, Tromsø, Hansine Hansens veg 18, 9019, Norway

E-mail: martin.rypdal@uit.no

ABSTRACT

A remaining carbon budget (RCB) estimates how much CO_2 we can emit and still reach a specific temperature target. The RCB concept is attractive since it easily communicates to the public and policymakers, but RCBs are also subject to uncertainties. The expected warming levels for a given carbon budget has a wide uncertainty range, which we show here to increase with less ambitious targets, i.e., with higher CO_2 emissions and temperatures. Leading causes of RCB uncertainty are the future non-CO_2 emissions, Earth system feedbacks, and the spread in the climate sensitivity among climate models. The latter is investigated in this paper, using simple emulators of Earth System Models in the Coupled Model Intercomparison Project Phase 6 (CMIP6) ensemble. It is shown that the transient climate response to cumulative emissions of carbon (TCRE) is approximately proportional to the effective equilibrium climate sensitivity (ECS). For temperature targets between 1.5-3.0°C, the models exhibiting low ECS increase RCB by a factor two compared to those with high sensitivity, suggesting that observational constraints imposed on the ECS in the model ensemble also will reduce uncertainty in the RCB estimates.

1. Introduction

The concept of remaining carbon budgets (RCBs) is appealing and highly applicable to climate mitigation policy. It allows us to relate a specific climate target to the remaining greenhouse gases humans can release into the atmosphere and still comply with this target. However, like all simple ideas in climate science, it demonstrates ambiguities and uncertainties. Ambiguities arise as the number of specific definitions of temperature targets and RCBs increase during efforts to make concepts and procedures precise. Uncertainties follow from these ambiguities and, more important, from the large spread in model projections, including those of state-of-the-art climate and Earth system models (ESMs). Notably, the spread across the ensemble of models and the corresponding uncertainties in their equilibrium climate sensitivity (ECS) and RCB do not seem to diminish with increasing model complexity. The state-of-the-art versions of ESMs included in the Coupled Model Intercomparison Project Phase 6 (CMIP6) show a span in ECS of 1.6–5.6 K with 10 models out of 27 exceeding 4.5 K (Zelinka et al. 2020). The increase in ECS is primarily linked to a stronger positive cloud feedback in some of the models, although this is still under investigation.

Unfortunately, the main advantage of the RCB concept as a policy tool, its appealing simplicity, tends to be lost in a plethora of specialized papers, and recent reviews (Rogelj et al. 2016, 2019) do not completely resolve this. Nevertheless, in spite of uncertainty and ambiguities, it is generally accepted that there is an approximate scenario independence in the relationship between the cumulative CO_2 emissions and the global mean surface temperature (GMST) over a considerable range of realistic mitigation scenarios (Rogelj et al. 2016, 2019; MacDougall and Friedlingstein 2015). More precisely, there is an approximately linear relationship between the GMST a given year and the cumulative emissions up to that year. Moreover, it turns out that in scenarios for

which the emissions drop to zero at a given year, the GMST will peak approximately that year, and hence the the peak GMST and the cumulative emissions up to the year of zero annual emissions satisfy the same linear relationship. The increase in GMST per unit of emitted CO_2 given by this linear relation is called the effective transient climate response to cumulative emissions of carbon (TCRE).

For illustration, we have computed GMST versus the cumulative emissions after 2018 using 86 emission scenarios from the Integrated Assessment Modeling Consortium & International Institute for Applied Systems Analysis (IIASA) (Huppmann et al. 2018). Details are given in Fig. 1a and Table 1. For those scenarios where annual emissions have dropped to zero a year in this century, we compute the cumulative emissions up to that year. For those scenarios where annual emissions are still positive in year 2100, we compute the cumulative emissions up to year 2100. The corresponding GMST values are evaluated for those years by means of the reduced-complexity model MAGICC (Model for the Assessment of Greenhouse-gas-Induced Climate Change, version 6.8) (Meinshausen et al. 2011a). GMST versus cumultaive emissions computed this way is plotted as the bullets shown in Fig. 1b. The slope of a straight line regressed to this plot serves as an estimate of TCRE based on this single climate model. We define a climate target as a particular GMST-value, e.g., 2.0 °C above the pre-industrial baseline, and the RCB for this target computed from MAGICC as the cumulative emissions for this GMST obtained from the regression line shown in Fig. 1b.

The transient climate response obtained by this procedure is the so-called *effective* TCRE (Matthews et al. 2017), since the emission scenarios applied to obtain the points in Fig. 1b contain other anthropogenic emissions than CO_2. The effective TCRE accounts for warming from other greenhouse gases than CO_2, most importantly methane, and for cooling effects due to atmospheric aerosols. In contrast, the CO_2-only TCRE is defined as the warming attributable to CO_2 forcing

alone. One can estimate the CO_2-only TCRE from ESM experiments, driven by atmospheric CO_2 concentration increases by 1% per year. The CO_2 emissions can be derived from the specified atmospheric CO_2 concentrations and the modeled atmosphere-ocean and atmosphere-land CO_2-fluxes, and hence the CO_2-only TCRE can be computed by dividing the GMST increase by the cumulative emissions. Using 15 CMIP5 models, Gillett et al. (2013) find CO_2-only TCRE in the range $0.22 - 0.65$°C per 1000 Gt CO_2, with a mean of 0.44°C per 1000 Gt CO_2.

Analyzing 11 CMIP6 models, Arora et al. (2020) found CO_2-only TCRE in the range $0.33 - 0.58$°C per 1000 Gt CO_2, with a mean of 0.44°C per 1000 Gt CO_2 (Table 2).

The basis of these estimates are scenarios where atmospheric CO_2 concentration increases by 1% per year, and not scenarios where we reduce emissions to mitigate climate change. The reason why this does not pose a problem is the above mentioned scenario-independence of the relation between the GMST and the cumulative emissions. The physical mechanism behind this scenario-indpendence is a subtle balancing of a delayed warming and cooling which both are scenario dependent, leaving to be realized the fraction of the warming that only depends on the total amount of CO_2 emitted. If all emitted CO_2 remained in the atmosphere (no sinks) some of the heating would be delayed due to the thermal inertia of the ocean, and more so in scenarios with high emissions. Thus, in this case, the warming realized would depend on the shape of the annual emission curve, and not only on the area under this curve. However, the net CO_2 take-up by the ocean and land biosphere will increase as atmospheric concentration increases, and the ESMs indicate that the reduced CO_2 forcing due to this uptake approximately offsets the additional forcing represented by the radiation imbalance due to the delayed warming of the ocean surface. Thus, there is effectively no delayed warming after the release of a lump of CO_2 or, in other words, all the warming from this lump is realized instantaneously. It also turns out that the warming is approximately proportional to the size of the lump and not strongly dependent on the background CO_2 concentration.

The implication is the linear dependence of GMST on cumulative emissions, and hence the GMST will not increase if the emissions stop; the temperature maximum will coincide with the time the annual emissions drop to zero (Matthews et al. 2017; MacDougall et al. 2020).

There are several ways of adjusting CO_2-only TCREs and RCBs to obtain their effective counterparts. One method is to estimate the fraction of the total radiative forcing attributable to anthropogenic CO_2-emissions. In the CMIP5 ensemble, the multi-model mean ratio of CO_2 forcing to total anthropogenic forcing has been estimated to be 0.86 (Meinshausen et al. 2011b; Matthews et al. 2017), which yields a multi-model mean effective TCRE of 0.51°C per 1000 Gt CO_2 based on the CO_2-only estimate of 0.44°C per 1000 Gt CO_2 (Gillett et al. 2013) .

Another approach (Matthews et al. 2017) is to estimate the effective TCRE by dividing the observed 1861-2015 GMST increase of 0.99°C by the 1870-2015 cumulative CO_2 emissions of 2035 Gt CO_2 to obtain TCRE $= 0.49$°C per 1000 Gt CO_2. However, in ambitious yet realistic future mitigation scenarios, where emissions are brought rapidly to zero in this century, the ratio of CO_2 forcing to total anthropogenic forcing may deviate from the historical estimates. In this case, it is necessary to make assumptions regarding the evolution in time of this ratio. The method applied in this paper is to analyze open source scenarios constructed using integrated assessment models (IAMs) (Huppmann et al. 2018) (Fig. 1a and Table 1). In these scenarios, the total CO_2 and methane emissions are known, and based on these we infer a simple quadratic model for the dependence between future CO_2 and methane emissions, and make assumptions on the evolution of aerosol emissions as greenhouse gas emissions are reduced to zero. We do not analyze the uncertainty in the future relationship between methane, aerosol, and CO_2 emissions. A quantification of this uncertainty would require predictions of climate mitigation policies, which is beyond the scope of this paper.

From the emission scenarios, we can obtain corresponding temperatures from an Earth system model of reduced complexity such as MAGICC (Meinshausen et al. 2011a). However, using a single climate model does not consider the large spread in climate model projections. To assess the uncertainties in RCBs, one should ideally explore an ensemble of realistic mitigation scenarios using the full set of ESMs in the CMIP6 ensemble, which is not feasible due to the computational costs. In this study, we construct emulators of ESMs in the CMIP6 ensemble based on $4\times CO_2$-runs of the models. We use impulse-response models to approximate how the atmospheric CO_2 concentrations depend on greenhouse gas emissions. From the emulators, we can analyze the relationship between cumulative emissions and peak temperatures, and estimate TCRE and RCBs. Our simple modeling set-up, described in Section 2, is based on generally accepted results from the climate modeling literature, while keeping them operational and straightforward.

2. Modelling set-up

We use a simple modeling set-up where atmospheric CO_2 concentrations are computed from emissions through an impulse response function describing the ratio of emitted CO_2 absorbed by land and ocean, the ratio that remains in the atmosphere, and the characteristic time scales of absorption. The form of the response function is derived from CO_2 pulse experiments in a carbon model intercomparison project (Joos et al. 2001). We make crude, and fixed, assumptions about how methane and aerosol emissions depend on CO_2 emissions, determine resulting concentrations as linear responses to CO_2 emissions, and then compute the global radiative forcing using standard relations described below. The GMST is finally computed from the radiative forcing using linear response models (essentially equivalent to three-box energy balance models (Fredriksen and Rypdal 2017)) with parameters fitted to $4\times CO_2$ experiments in ESMs. (See Fig.2). These box models work as emulators of the ESMs for GSMT.

We model the concentrations of CO_2 and methane as linear responses of scenario data for emissions, $E_{CO_2}(t)$ and $E_{CH_4}(s)$:

$$[CO_2] = 280\,\text{ppm} + \int_{t_0}^{t} G_{CO_2}(t-s)E_{CO_2}(s)\,ds\,,$$

and

$$[CH_4] = 700\,\text{ppb} + \int_{t_0}^{t} G_{CH_4}(t-s)E_{CH_4}(s)\,ds\,.$$

The time t_0 refers to the year 1750, and the concentrations 280 ppm and 700 ppb are the preindustrial concentrations of CO_2 and methane, respectively. The impulse response function for CO_2 is of the form

$$G_{CO_2}(t) = c_0 + \sum_{i=1}^{4} c_i e^{-t/\tau_i}\,.$$

We use the results for the CO_2 fraction remaining in the atmosphere from 1 to 1000 years after a 100 GtC pulse from the CO_2 impulse experiments (Joos et al. 2001) to calibrate this response function. Parameters for the impulse response functions are obtained by fitting to the multi-model mean and the curves for the mean plus/minus one standard deviation. For the multi-model mean we find

$$\begin{aligned} c_0 &= 0.128 \text{ Gt } CO_2 \text{ per yr} \\ c_1 &= 0.019 \text{ Gt } CO_2 \text{ per yr} \\ c_2 &= 0.032 \text{ Gt } CO_2 \text{ per yr} \\ c_3 &= 0.035 \text{ Gt } CO_2 \text{ per yr} \\ c_4 &= 0.025 \text{ Gt } CO_2 \text{ per yr} \end{aligned} \tag{1}$$

The fit to the multi-model mean plus one standard deviation gives parameters

$$\begin{aligned} c_0 &= 0.128 \text{ Gt } CO_2 \text{ per yr} \\ c_1 &= 0.014 \text{ Gt } CO_2 \text{ per yr} \\ c_2 &= 0.071 \text{ Gt } CO_2 \text{ per yr} \\ c_3 &= 0.040 \text{ Gt } CO_2 \text{ per yr} \\ c_4 &= 0.033 \text{ Gt } CO_2 \text{ per yr} \end{aligned} \tag{2}$$

and the multi-model mean minus one standard deviation gives parameters

$$\begin{aligned} c_0 &= 0.128 \text{ Gt } CO_2 \text{ per yr} \\ c_1 &= 0.023 \text{ Gt } CO_2 \text{ per yr} \\ c_2 &= 0.038 \text{ Gt } CO_2 \text{ per yr} \\ c_3 &= 0.033 \text{ Gt } CO_2 \text{ per yr} \\ c_4 &= 0.019 \text{ Gt } CO_2 \text{ per yr} \end{aligned} \tag{3}$$

Methane concentration is modeled using a response function $G_{CH_4}(t) = c\,e^{-t/\tau}$ with $c = 0.34$ ppb/(Mt CH_4 per yr) and $\tau = 12.3$ yrs. The factor c is chosen to yield the observed atmospheric methane concentration in 2019 of 1880 ppb and based on the emissions since 1750. We model methane emissions to be proportional to CO_2 emissions before 2018: $E_{CH_4}(t) = aE_{CO_2}(t)$ with $a =$ 11.9 (ppb CH_4)/(ppm CO_2) (Boden et al. 2017; Saunois et al. 2020). After 2018 we assume a quadratic relationship fitted to the empirical relationship between CO_2 and methane emissions in the scenario data base (Huppmann et al. 2018). (See Fig. 3). The quadratic relationship ensures that methane emissions remain positive even if CO_2 emissions become negative.

Forcing is computed from emissions using the approach of Myhre et al. (1998): The radiative forcing associated with atmospheric CO_2 is

$$F_{CO_2} = \frac{F_{2\times CO_2}}{\log 2} \log\left(1 + \frac{[CO_2] - 280\,\text{ppm}}{280\,\text{ppm}}\right),$$

where $F_{2\times CO_2}$ is the forcing associated with a CO_2-doubling. This number is model-dependent and obtained from the Gregory plots for the abrupt $4\times CO_2$ experiments in the CMIP6 ensemble (Gregory et al. 2004). The radiative forcing associated with atmospheric methane is modelled as

$$F_{CH_4} = p\left(\sqrt{\frac{[CH_4]}{\mu}} - \sqrt{\frac{700\,\text{ppm}}{\mu}}\right),$$

where $\mu = 1\,\text{ppm}$ and $p = 0.036\,\text{W/m}^2$ describes the potential of methane as a greenhouse gas. Aerosol forcing is assumed to be negative with magnitude proportional to CO_2 emissions but assumed not to go below $-0.4\,\text{W/m}^2$ as emissions are reduced:

$$F_{\text{aero}} = \begin{cases} bE_{CO_2} & \text{if } E_{CO_2} > 20 \text{ Gt } CO_2 \text{ per yr} \\ -0.4 \text{ W/m}^2 & \text{otherwise} \end{cases},$$

with $b = -0.02$ W/m^2 per Gt CO_2 obtained from the ratio between CO_2 forcing and aerosol forcing since the preindustrial period (Hansen et al. 2005). Our analyses show that the overall conclusions of this study are not sensitive to the assumed aerosol forcing of -0.4 W/m^2 after reaching net-zero emissions.

Our model for GMST is

$$T(t) = \int_{t_0}^{t} G_T(t-s) F_{\text{tot}}(s) ds,$$

with $F_{\text{tot}} = F_{\text{CO}_2} + F_{\text{CH}_4} + F_{\text{aero}}$ and

$$G_T(t) = \sum_{i=1}^{3} d_i e^{-t/\tau_i} .$$

The time scales τ_i are chosen to be 1, 10, and 100 yrs, and the factors d_i are estimated from the first 150 yrs in $4\times\text{CO}_2$ experiments in CMIP6 using linear regression (Fig. 2). The results are not sensitive to the choice of time scales (Fredriksen and Rypdal 2017), but the slow climate response, in this case the parameter d_3, is not well constrained by 150-yr runs (Sanderson 2020). On the other hand, the analyses in presented in this paper only concern GMST up to the year 2100, and are insensitive to this uncertainty.

Table 3 shows the estimated parameters d_1, d_2, and d_3 for the 41 models in the CMIP6 ensemble. The table also shows the ECS and $F_{2\times\text{CO}_2}$ of each climate model, estimated using the standard Gregory-plot technique (Gregory et al. 2004).

Using the updated HadCrut data set we set the current GMST at 1.1°C above the 1850-1900 baseline (Morice et al. 2012).

Results

Our ESM emulators show that the linear relationship between total emissions and maximum GMST is an excellent approximation for each climate model, but that the TCRE varies considerably over the model ensemble (Fig. 4a). Using the carbon impulse response fitted to the multi-model mean in the ensemble of Joos et al. (2001) we find mean TCRE for peak warming of 0.58°C per 1000 Gt CO2, with a 66% likely range of 0.46-0.73°C per 1000 Gt CO2 (See the histogram and the solid black curve in Fig. 4b). Using the upper and lower ranges of CO_2 concentrations in the ensemble of CO_2-pulse simulations (Joos et al. 2001), i.e. plus/minus one standard deviation, we find mean TCREs for peak warming of 0.63°C and 0.53°C per 1000 Gt CO2, respectively. The

66% likely ranges are 0.42-0.66°C per 1000 Gt CO2 and 0.49-0.78°C per 1000 Gt CO2 (see the dashed and dotted curves in Fig. 4b). From Fig. 4a we can produce histograms for the 1.5, 2.0, 2.5, and 3.0°C climate targets (Fig. 5) and this allows us to compute confidence ranges for the RCB for each target. We can also compute the RCBs that give a 50% (or 66%) chance to meet the target (Table 4).

The estimated TCRE for peak warming correlates strongly with the effective ECS of the ESMs estimated from 150 yrs of data in $4\times CO_2$-runs (Fig. 6a). The correlation coefficient is $\rho = 0.94$, and the statistical significance is $p = 10^{-19}$. The estimated relationship is

$$\mathrm{TCRE} = A + B\,\mathrm{ECS}\,,$$

with $A = 0.2$ °C per 1000 Gt CO2 and $B = 0.1$ °C per K per 1000 Gt CO2. The ECS ranges from 1.8 to 5.6 K in the CMIP6 ensemble, corresponding to a range of 0.4 to 0.8°C per 1000 Gt CO2 in TCRE. The RCB for a given peak temperature target varies by a factor of two over the model ensemble.

For the climate models with ECS > 4.0 K, the mean TCRE for peak warming is 0.71°C per 1000 Gt CO2, with a 66% likely range of 0.66-0.77°C per 1000 Gt CO2. For the climate models with ECS < 4.0 K, the mean TCRE for peak warming is 0.51°C per 1000 Gt CO2, with a 66% likely range of 0.44-0.59°C per 1000 Gt CO2. The corresponding difference in RCB grows linearly with the temperature target (Fig. 6b and Fig. 7).

We observe that over the ensemble of scenarios, the multi-model mean GMST response of the CMIP6 emulators align closely with the estimates from the MAGICC model (Fig. 8).

The TCRE estimates obtained in this study are consistent with the CO_2-only TCREs found by Arora et al. (2020). Nine of the eleven CMIP6 models they analyzed are included here, and for

these models, the correlation between their CO_2-only TCRE estimates and our emulator-based TCRE estimates is 0.89 ($p = 0.0001$) (Table 2).

Discussion

Our analyses show that besides the uncertainty in future emissions of methane and aerosols, estimates of RCBs are associated with considerable uncertainty related to the global temperature response to radiative forcing, quantified for example as the spread over different members of the CMIP6 model ensemble. We further show that model estimates of TCRE correlate strongly with climate sensitivity. Arora et al. (2020) compare CO_2-only estimates of TCRE with estimates of the transient climate response (TCR), and in this paper we obtain similar results for the relationship between TCRE and effective ECS, which is not surprising since effective ECS and TCR correlate significantly (Yoshimori et al. 2016). It is convenient to use effective ECS as a proxy for TCRE, and hence for RCB, since much effort is being made to use observations to constrain the ECS obtained from ESMs. Cox et al. (2018) used the instrumental temperature record to constrain ECS in the CMIP5 ensemble to a 66% confidence interval of 2.2–3.4 K. This approach was based on an assumed theoretical relation between ECS and unforced temperature temperature fluctuations, whereas the analysis reflected the forced temperature responses (Rypdal et al. 2018; Po-Chedley et al. 2018; Brown et al. 2018). To circumvent this issue, Jiménez-de-la Cuesta and Mauritsen (2019) used observational data of post 1970 warming to constrain ECS in the CMIP5 ensemble to a 95% confidence interval of 1.72–4.12 K. This result is roughly consistent with the recent results of Sherwood et al. (2020), who used multiple lines of evidence to argue that ECS above 4.5 K is unlikely. Including an observational constraint on ECS would narrow the TCRE uncertainty presented in this paper. An alternative, but related, approach is to tune emulators to observational data (Smith et al. 2018).

The estimated uncertainty in TCRE corresponds directly to the uncertainty in RCB, which we find to depend linearly on the GMST target. Hence, the less ambitious the temperature target, the higher the uncertainty in the corresponding RCB.

Since we use linear emulators and fixed impulse-response carbon model, there is an additional source of uncertainty that is not accounted for, induced by positive feedbacks in the dynamics of the Earth system. For example, carbon-climate feedbacks and carbon-concentration feedbacks have been shown to be a significant source of uncertainty for RCBs (Jones and Friedlingstein 2020). Permafrost thawing in response to rising surface temperatures leads to the release of greenhouse gases stored in high-latitude soils. The release of these additional greenhouse gases will in turn accelerate global warming.

The Amazon rainforest is another example of such a positive feedback. It has been argued and observed in climate model projections that the Amazon ecosystem might transition from its current rainforest state to a state dominated by grassland and savanna vegetation (Cox et al. 2004; Hirota et al. 2011; Lovejoy and Nobre 2018, 2019) which would be accompanied by the release of large amounts of carbon dioxide to the atmosphere. Carbon-cycle feedbacks have an overall accelerating effect on global warming (Cox et al. 2000), and the situation seems particularly evident for the Amazon. Increasing tree mortality during a transition from rainforest to Savanna will cause the rainforest to turn from a global carbon sink to a global source of carbon (Brienen et al. 2015), as has already happened temporarily during the severe droughts of 2005 and 2010 (Feldpausch et al. 2016). Climate-change-induced dieback of the Amazon would lead to the release of additional greenhouse gases, which would further accelerate global temperature rise.

The Amazon rainforest also provides an example of how anthropogenic forcing other than greenhouse gas release can affect the climate system. Modelling evidence suggests that only partial deforestation of the Amazon rainforest might – through intricate couplings between evapotran-

spiration, condensational latent heating, and the South American low-level circulation system – lead to a collapse of the South American monsoon system and thus, ultimately, of the Amazon rainforest (Boers et al. 2017).

As a third example, the ice-albedo feedback implies rising temperatures in the Arctic, leading to accelerating sea ice retreat, lowering albedo, and effectively increasing mean surface temperatures regionally. This positive feedback contributes to uncertainty in TCRE, which translates to even more considerable uncertainty in the amount of greenhouse gas emissions we can allow to still limit peak temperature to specified targets.

These three examples of positive Earth system feedbacks are all – in some form – implemented in state-of-the-art models such as the ones from the CMIP6 suite (Eyring et al. 2016), and systematic searches have revealed many abrupt transitions related to such positive feedbacks in model projections (Drijfhout et al. 2015). Nevertheless, it is still assumed that state-of-the-art models remain too stable (Valdes 2011). The presence of positive feedbacks and potential tipping points within the Earth system adds a layer of uncertainty to RCBs that is extremely difficult to quantify.

Acknowledgments. This project has received funding from the European Union's Horizon 2020 research and innovation program under grant agreement No. 820970 (TiPES). It was also supported by the UiT Aurora Center Program, UiT The Arctic University of Norway (2020). N.B. acknowledges funding from the Volkswagen foundation.

References

Arora, V. K., and Coauthors, 2020: Carbon–concentration and carbon–climate feedbacks in cmip6 models and their comparison to cmip5 models. *Biogeosciences*, **17 (16)**, 4173–4222, doi:10.5194/bg-17-4173-2020, URL https://bg.copernicus.org/articles/17/4173/2020/.

Boden, T., G. Marland, and R. J. Andres, 2017: Global, regional, and national fossil-fuel co2 emissions (1751 - 2014). *Carbon Dioxide Information Analysis Center (CDIAC), Oak Ridge National Laboratory (ORNL)*, **V. 2017**, , doi:10.3334/CDIAC/00001_V2017.

Boers, N., N. Marwan, H. M. J. Barbosa, and J. Kurths, 2017: A deforestation-induced tipping point for the south american monsoon system. *Scientific Reports*, **7 (1)**, 41 489, doi:10.1038/srep41489.

Brienen, R. J. W., and Coauthors, 2015: Long-term decline of the amazon carbon sink. *Nature*, **519 (7543)**, 344–348, doi:10.1038/nature14283.

Brown, P. T., M. B. Stolpe, and K. Caldeira, 2018: Assumptions for emergent constraints. *Nature*, **563 (7729)**, E1–E3, doi:10.1038/s41586-018-0638-5.

Cox, P. M., R. A. Betts, M. Collins, P. P. Harris, C. Huntingford, and C. D. Jones, 2004: Amazonian forest dieback under climate-carbon cycle projections for the 21st century. *Theoretical and Applied Climatology*, **78 (1)**, 137–156, doi:10.1007/s00704-004-0049-4.

Cox, P. M., R. A. Betts, C. D. Jones, S. A. Spall, and I. J. Totterdell, 2000: Acceleration of global warming due to carbon-cycle feedbacks in a coupled climate model. *Nature*, **408 (6809)**, 184–187, doi:10.1038/35041539.

Cox, P. M., C. Huntingford, and M. S. Williamson, 2018: Emergent constraint on equilibrium climate sensitivity from global temperature variability. *Nature*, **553 (7688)**, 319–322, doi:10.1038/nature25450, URL https://doi.org/10.1038/nature25450.

Drijfhout, S., and Coauthors, 2015: Catalogue of abrupt shifts in intergovernmental panel on climate change climate models. *Proceedings of the National Academy of Sciences*, **112 (43)**, E5777–E5786, doi:10.1073/pnas.1511451112.

Eyring, V., S. Bony, G. A. Meehl, C. A. Senior, B. Stevens, R. J. Stouffer, and K. E. Taylor, 2016: Overview of the coupled model intercomparison project phase 6 (cmip6) experimental design and organization. *Geoscientific Model Development*, **9 (5)**, 1937–1958, doi:10.5194/gmd-9-1937-2016, URL https://gmd.copernicus.org/articles/9/1937/2016/.

Feldpausch, T. R., and Coauthors, 2016: Amazon forest response to repeated droughts. *Global Biogeochemical Cycles*, **30 (7)**, 964–982, doi:10.1002/2015GB005133.

Fredriksen, H.-B., and M. Rypdal, 2017: Long-Range Persistence in Global Surface Temperatures Explained by Linear Multibox Energy Balance Models. *Journal of Climate*, **30 (18)**, 7157–7168, doi:10.1175/JCLI-D-16-0877.1.

Gillett, N. P., V. K. Arora, D. Matthews, and M. R. Allen, 2013: Constraining the Ratio of Global Warming to Cumulative CO2 Emissions Using CMIP5 Simulations*. *Journal of Climate*, **26 (18)**, 6844–6858, doi:10.1175/JCLI-D-12-00476.1.

Gregory, J. M., and Coauthors, 2004: A new method for diagnosing radiative forcing and climate sensitivity. *Geophysical Research Letters*, **31 (3)**, doi:10.1029/2003GL018747.

Hansen, J., and Coauthors, 2005: Efficacy of climate forcings. *Journal of Geophysical Research: Atmospheres*, **110**, D18 104, doi:10.1029/2005JD005776.

Hirota, M., M. Holmgren, E. H. Van Nes, and M. Scheffer, 2011: Global resilience of tropical forest and savanna to critical transitions. *Science*, **334 (6053)**, 232–235, doi:10.1126/science.1210657.

Huppmann, D., and Coauthors, 2018: Iamc 1.5°C scenario explorer and data hosted by iiasa. URL https://data.ene.iiasa.ac.at/iamc-sr15-explorer, doi:10.22022/SR15/08-2018.15429.

Jiménez-de-la Cuesta, D., and T. Mauritsen, 2019: Emergent constraints on earth's transient and equilibrium response to doubled co2 from post-1970s global warming. *Nature Geoscience*, **12 (11)**, 902–905, doi:10.1038/s41561-019-0463-y, URL https://doi.org/10.1038/s41561-019-0463-y.

Jones, C. D., and P. Friedlingstein, 2020: Quantifying process-level uncertainty contributions to TCRE and carbon budgets for meeting paris agreement climate targets. *Environmental Research Letters*, **15 (7)**, 074 019, doi:10.1088/1748-9326/ab858a, URL https://doi.org/10.1088/1748-9326/ab858a.

Joos, F., I. C. Prentice, S. Sitch, R. Meyer, G. Hooss, G.-K. Plattner, S. Gerber, and K. Hasselmann, 2001: Global warming feedbacks on terrestrial carbon uptake under the intergovernmental panel on climate change (ipcc) emission scenarios. *Global Biogeochemical Cycles*, **15 (4)**, 891–907.

Lovejoy, T. E., and C. Nobre, 2018: Amazon tipping point. *Science Advances*, **4 (2)**, doi:10.1126/sciadv.aat2340.

Lovejoy, T. E., and C. Nobre, 2019: Amazon tipping point: Last chance for action. *Science Advances*, **5 (12)**, doi:10.1126/sciadv.aba2949.

MacDougall, A. H., and P. Friedlingstein, 2015: The Origin and Limits of the Near Proportionality between Climate Warming and Cumulative CO2 Emissions. *Journal of Climate*, **28 (10)**, 4217–4230, doi:10.1175/JCLI-D-14-00036.1.

MacDougall, A. H., and Coauthors, 2020: Is there warming in the pipeline? a multi-model analysis of the zero emissions commitment from co2. *Biogeosciences*, **17 (11)**, 2987–3016, doi:10.5194/bg-17-2987-2020, URL https://bg.copernicus.org/articles/17/2987/2020/.

Matthews, H. D., J.-S. Landry, A.-I. Partanen, M. Allen, M. Eby, P. M. Forster, P. Friedlingstein, and K. Zickfeld, 2017: Estimating carbon budgets for ambitious climate targets. *Current Climate Change Reports*, **3 (1)**, 69–77, doi:10.1007/s40641-017-0055-0.

Meinshausen, M., S. C. Raper, and T. M. Wigley, 2011a: Emulating coupled atmosphere-ocean and carbon cycle models with a simpler model, magicc6-part 1: Model description and calibration.

Meinshausen, M., and Coauthors, 2011b: The rcp greenhouse gas concentrations and their extensions from 1765 to 2300. *Climatic Change*, **109 (1)**, 213, doi:10.1007/s10584-011-0156-z.

Morice, C. P., J. J. Kennedy, N. A. Rayner, and P. D. Jones, 2012: Quantifying uncertainties in global and regional temperature change using an ensemble of observational estimates: The hadcrut4 data set. *Journal of Geophysical Research: Atmospheres*, **117 (D8)**, doi:https://doi.org/10.1029/2011JD017187, URL https://agupubs.onlinelibrary.wiley.com/doi/abs/10.1029/2011JD017187, https://agupubs.onlinelibrary.wiley.com/doi/pdf/10.1029/2011JD017187.

Myhre, G., E. J. Highwood, K. P. Shine, and F. Stordal, 1998: New estimates of radiative forcing due to well mixed greenhouse gases. *Geophysical research letters*, **25 (14)**, 2715–2718.

Po-Chedley, S., C. Proistosescu, K. C. Armour, and B. D. Santer, 2018: Climate constraint reflects forced signal. *Nature*, **563 (7729)**, E6–E9, doi:10.1038/s41586-018-0640-y, URL https://doi.org/10.1038/s41586-018-0640-y.

Rogelj, J., P. M. Forster, E. Kriegler, C. J. Smith, and R. Séférian, 2019: Estimating and tracking the remaining carbon budget for stringent climate targets. *Nature*, **571 (7765)**, 335–342, doi:10.1038/s41586-019-1368-z.

Rogelj, J., M. Schaeffer, P. Friedlingstein, N. P. Gillett, D. P. van Vuuren, K. Riahi, M. Allen, and R. Knutti, 2016: Differences between carbon budget estimates unravelled. *Nature Climate Change*, **6**, 245, doi:10.1038/nclimate2868.

Rypdal, M., H.-B. Fredriksen, K. Rypdal, and R. J. Steene, 2018: Emergent constraints on climate sensitivity. *Nature*, **563 (7729)**, E4–E5, doi:10.1038/s41586-018-0639-4.

Sanderson, B., 2020: Relating climate sensitivity indices to projection uncertainty. *Earth System Dynamics*, **11 (3)**, 721–735, doi:10.5194/esd-11-721-2020, URL https://esd.copernicus.org/articles/11/721/2020/.

Saunois, M., and Coauthors, 2020: The global methane budget 2000–2017. *Earth System Science Data*, **12 (3)**, 1561–1623, doi:10.5194/essd-12-1561-2020, URL https://essd.copernicus.org/articles/12/1561/2020/.

Sherwood, S., and Coauthors, 2020: An assessment of earth's climate sensitivity using multiple lines of evidence. *Reviews of Geophysics*, **n/a (n/a)**, e2019RG000 678, doi:10.1029/2019RG000678.

Smith, C. J., P. M. Forster, M. Allen, N. Leach, R. J. Millar, G. A. Passerello, and L. A. Regayre, 2018: Fair v1.3: a simple emissions-based impulse response and carbon cycle model.

Geoscientific Model Development, **11 (6)**, 2273–2297, doi:10.5194/gmd-11-2273-2018, URL https://gmd.copernicus.org/articles/11/2273/2018/.

Valdes, P., 2011: Built for stability. *Nature Geoscience*, **4 (7)**, 414–416, doi:10.1038/ngeo1200.

Yoshimori, M., M. Watanabe, H. Shiogama, A. Oka, A. Abe-Ouchi, R. Ohgaito, and Y. Kamae, 2016: A review of progress towards understanding the transient global mean surface temperature response to radiative perturbation. *Progress in Earth and Planetary Science*, **3 (1)**, 21, doi:10.1186/s40645-016-0096-3, URL https://doi.org/10.1186/s40645-016-0096-3.

Zelinka, M. D., T. A. Myers, D. T. McCoy, S. Po-Chedley, P. M. Caldwell, P. Ceppi, S. A. Klein, and K. E. Taylor, 2020: Causes of higher climate sensitivity in cmip6 models. *Geophysical Research Letters*, **47 (1)**, e2019GL085 782, doi:10.1029/2019GL085782.

LIST OF TABLES

	AIM/CGE	GCAM4	IMAGE	MESSAGE-GLOBIOM	REMIND-MAGPIE	WITCH-GLOBIOM
SSP1-19	✓	✓	✓	✓	✓	✓
SSP1-26	✓	✓	✓	✓	✓	✓
SSP1-34	✓	✓	✓	✓	✓	✓
SSP1-45	✓	✓	✓	✓	✓	✓
SSP1-Baseline	✓		✓		✓	
SSP2-19	✓	✓		✓	✓	
SSP2-26	✓	✓	✓	✓	✓	✓
SSP2-34	✓	✓	✓	✓	✓	✓
SSP2-45	✓	✓	✓	✓	✓	✓
SSP3-34	✓		✓	✓		✓
SSP3-45	✓		✓	✓		✓
SSP3-60	✓					
SSP4-19						✓
SSP4-26	✓	✓	✓			✓
SSP4-34	✓	✓	✓			✓
SSP4-45	✓	✓	✓			✓
SSP5-19		✓			✓	
SSP5-26	✓	✓			✓	
SSP5-34	✓	✓	✓		✓	✓
SSP5-45	✓	✓	✓		✓	✓

TABLE 1. The Shared Socioeconomic Pathways (SSPs) and integrated assessment models (IAMs) that form the 86 emission scenarios shown in Fig. 1a.

TABLE 2. Comparison with the results of Arora et al. (2020).

CMIP6 model	CO_2-only TCRE (°C per 1000 Gt CO_2) (Arora et al. 2020)	TCRE (°C per 1000 Gt CO_2) Emulators	TCR (K) (Arora et al. 2020)	ECS (K)
ACCESS-ESM1.5	0.50	0.57	2.15	4.7
BCC-CSM2-MR	0.33	0.54	1.70	3.0
CanESM5	0.52	0.79	2.54	5.6
CESM2	0.53	0.75	2.29	5.2
CNRM-ESM2-1	0.41		1.84	
IPSL-CM6A-LR	0.53	0.73	2.36	4.6
MIROC-ES2L	0.35	0.45	1.58	2.7
MPI-ESM1.2-LR	0.41	0.53	1.86	3.0
NOAA-GFDL-ESM4	0.36		1.55	.
NorESM2-LM	0.33	0.48	1.42	2.6
UKESM1-0-LL	0.57	0.77	2.42	5.4

Earth System Model	d_1 (K m^2/W yrs)	d_2 (K m^2/W yrs)	d_3 (K m^2/W yrs)	ECS (K)	$F_{2\times CO_2}$ (W m^{-2})
ACCESS-CM2	0.25	0.041	0.004	4.7	3.4
ACCESS-ESM1-5	0.28	0.034	0.005	3.9	2.8
AWI-CM-1-1-MR	0.28	0.028	0.003	3.2	3.6
BCC-CSM2-MR	0.36	0.016	0.003	3.0	3.1
BCC-ESM1	0.24	0.037	0.003	3.3	3.0
CAMS-CSM1-0	0.22	0.020	0.001	2.3	4.2
CanESM5	0.20	0.055	0.004	5.6	3.7
CAS-ESM2-0	0.34	0.029	0.003	3.5	3.3
CESM2	0.34	0.028	0.006	5.2	3.3
CESM2-FV2	0.38	0.027	0.006	5.2	2.9
CESM2-WACCM	0.30	0.031	0.005	4.7	3.3
CESM2-WACCM-FV2	0.30	0.036	0.005	4.8	2.9
CMCC-CM2-SR5	0.22	0.038	0.002	3.5	3.8
CNRM-CM6-1	0.23	0.050	0.003	4.9	3.6
CNRM-CM6-1-HR	0.19	0.046	0.002	4.3	4.0
E3SM-1-0	0.18	0.068	0.006	5.3	3.3
EC-Earth3-Veg	0.24	0.045	0.005	4.3	3.4
FGOALS-f3-L	0.28	0.019	0.002	3.0	4.1
FGOALS-g3	0.29	0.017	0.002	2.8	3.7
GFDL-CM4	0.35	0.027	0.004	3.9	3.2
GFDL-ESM4	0.25	0.025	0.001	2.6	3.8
GISS-E2-1-G	0.31	0.017	0.001	2.8	3.6
GISS-E2-1-H	0.25	0.028	0.002	3.1	3.5
GISS-E2-2-G	0.23	0.026	0.000	2.4	3.7
IITM-ESM	0.23	0.013	0.001	2.4	4.6
INM-CM4-8	0.30	0.019	0.002	1.8	2.7
INM-CM5	0.23	0.026	0.001	1.9	2.9
IPSL-CM6A-LR	0.23	0.051	0.004	4.6	3.4
KACE-1-0-G	0.19	0.033	0.004	4.4	3.3
MIROC-ES2L	0.20	0.025	0.001	2.7	4.1
MIROC6	0.24	0.023	0.001	2.6	3.7
MPI-ESM1-2-HR	0.29	0.018	0.003	3.0	3.6
MPI-ESM1-2-LR	0.23	0.025	0.001	3.0	4.2
MRI-ESM2-0	0.30	0.017	0.003	3.1	3.5
NESM3	0.40	0.033	0.003	4.8	3.7
NorCPM1	0.25	0.023	0.003	3.0	3.3
NorESM2-LM	0.40	0.002	0.002	2.6	3.4
NorESM2-MM	0.35	0.006	0.002	2.5	3.8
SAM0-UNICON	0.30	0.024	0.002	3.7	3.9
TaiESM1	0.26	0.034	0.003	4.3	4.0
UKESM1-0-LL	0.22	0.052	0.005	5.4	3.6

421 TABLE 3. Estimates of ECS, forcing and linear-response parameters in CMIP6 models for each emission
422 scenario. Time constants are fixed as 1 yr, 10 yrs, and 100 yrs.

TABLE 4. Estimated RCBs based on the emulators of ESMs in the CMIP6 ensemble.

Target (°C)	50%-chance RCB (Gt CO_2)	66%-chance RCB (Gt CO_2)
1.5	421	330
2.0	1274	1119
2.5	2168	1920
3.0	3064	2721

LIST OF FIGURES

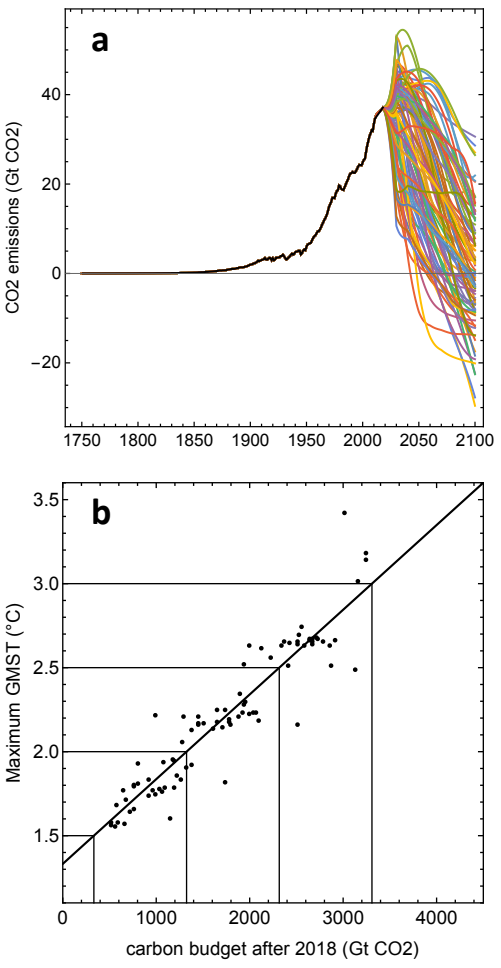

FIG. 1. Emission scenarios and RCB estimates from the MAGICC model. (a) The 86 emission scenarios analyzed in this paper. They are collected from the Integrated Assessment Modeling Consortium & International Institute for Applied Systems Analysis (IIASA) (Huppmann et al. 2018) . (b) The plot shows peak GMST versus cumulative positive emissions after 2018 evaluated by the MAGICC model. The lines explicitly show the RCBs for this particular model, for the GMST targets 1.5, 2, 2.5, and 3°C.

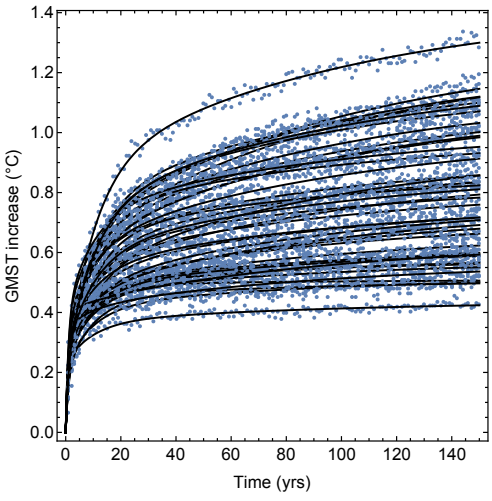

FIG. 2. ESM emulators in the CMIP6 ensemble fitted to $4\times CO_2$ runs. The points show the temperature increase over the first 150 yrs after an abrupt quadrupling of CO_2 normalized by dividing by the Gregory-estimate of the forcing. The black curves are the fitted temperature responses as described in the Methods section.

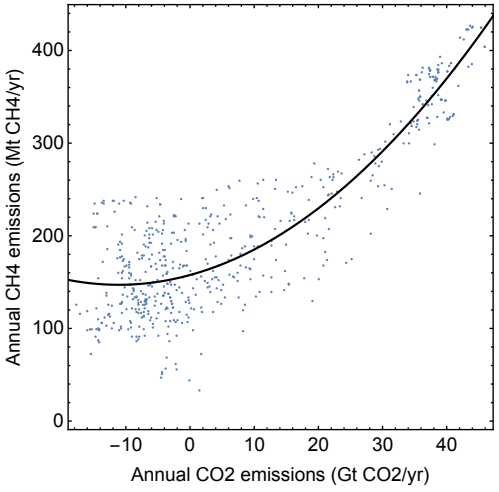

FIG. 3. The dependence between CO_2 and methane emissions in the scenario database. The points show the annual methane emissions versus the annual CO_2 emissions for each emission scenario and each year from 2018 to 2100. The curve show a quadratic fit to the points.

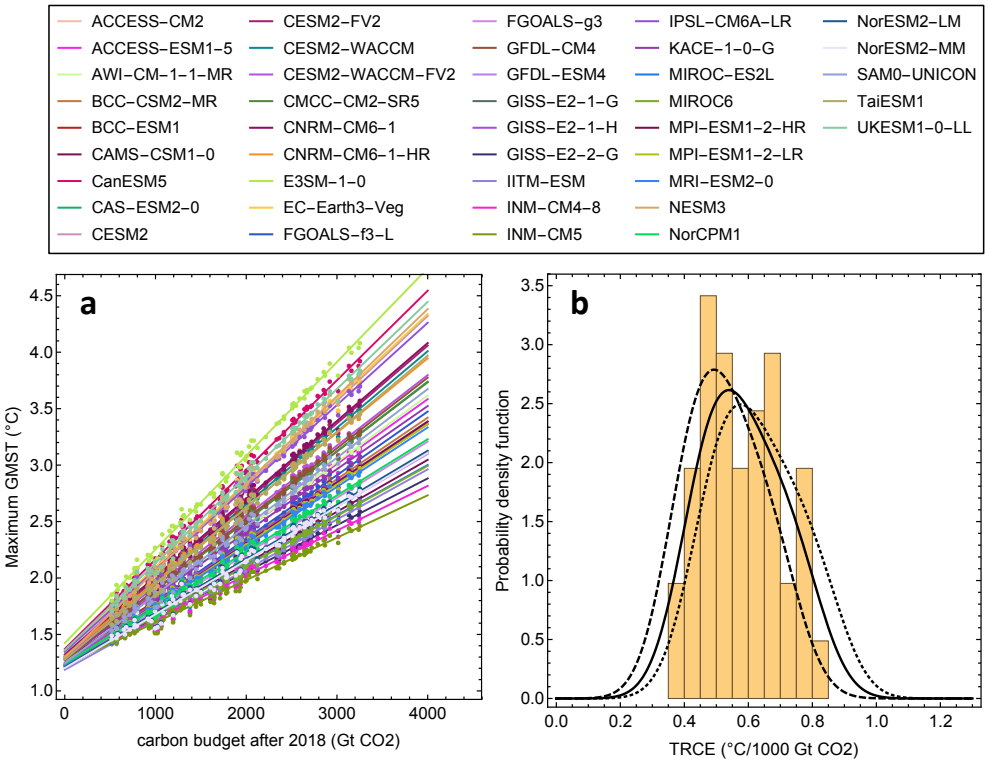

FIG. 4. Estimates of TRCE from CMIP6 emulators. (a) Shows the approximately linear relationship between total positive CO_2 emissions between 2018 and 2100 and the maximum GMST for 86 emission scenarios and evaluated with emulators of 41 different climate models in the CMIP6 ensemble. Each color represents a climate model and each point an emission scenario. The lines are fitted for each model using linear regression. (b) The histogram shows the distribution of the TCRE obtained from the slopes of the linear fits in Fig. 2a for the 41 different climate model emulators. The solid curve is a smooth kernel estimate of the probability density. The dotted and dashed curves are the estimated probability densities for the TCRE when we use the upper- and lower ranges (model mean plus/minus one standard deviation) of the impulse-response carbon model.)

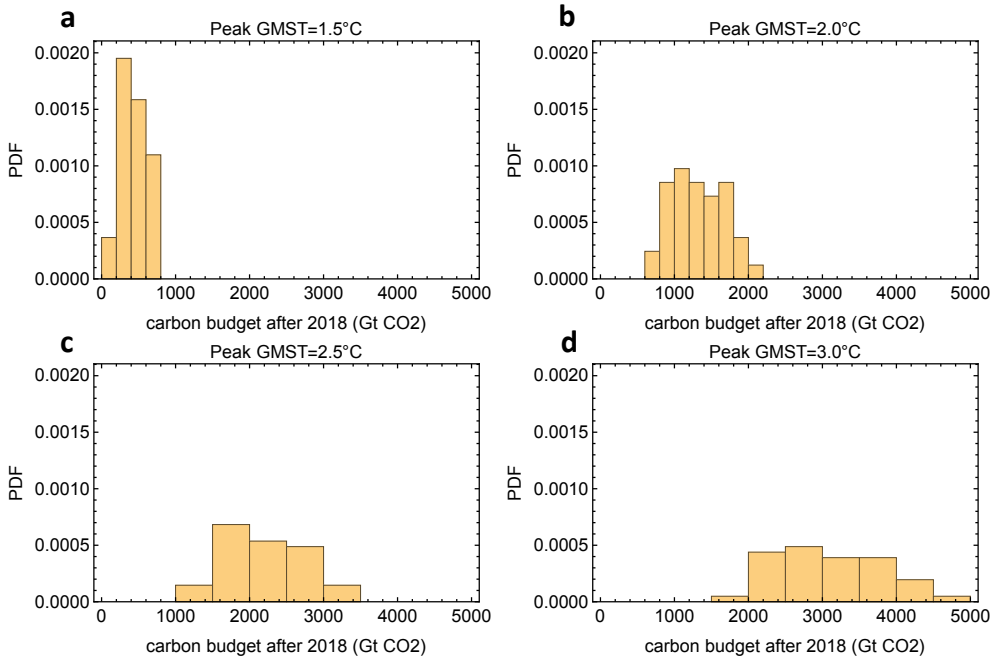

484 FIG. 5. Estimates of RCB for different temperature targets. (a)-(d) show histograms for the 1.5, 2.0, 2.5, and
485 3.0 °C-targets, respectively.

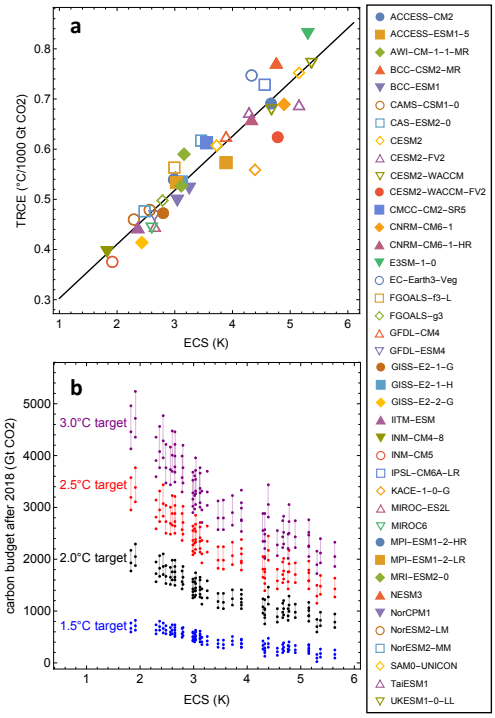

FIG. 6. The relationship between RCBs and ECS in the CMIP6 ESM emulators. (a) Shows the approximately linear relationship between the TCRE of the ESM emulators and the ECS estimated from Gregory-plots for 41 models in CMIP6. (b) Shows the RCBs for different maximum GMST targets as against the ECS of the climate model. The points are obtained using the multi-model mean impulse-response carbon model and the upper- and lower ranges (multi-model mean plus/minus one standard deviation).

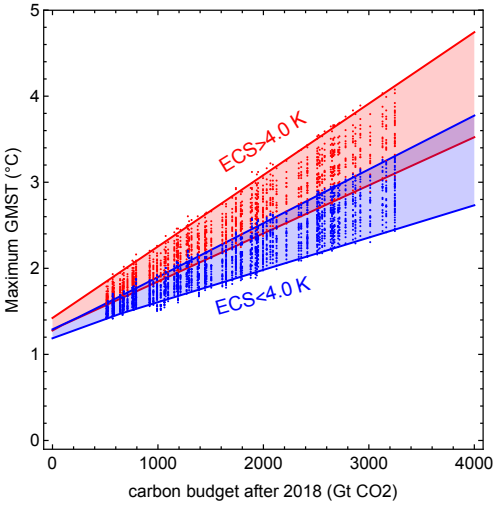

FIG. 7. Linear relationships between total positive CO_2 emissions and peak GMST for models with high- and low ECS. Shows the same data as in Fig. 4a, but colored so that models with ECS>4.0 K are in red and models with ECS<4.0 K are in blue. The lines show the minimum and maximum TCRE for the two ranges of ECS.

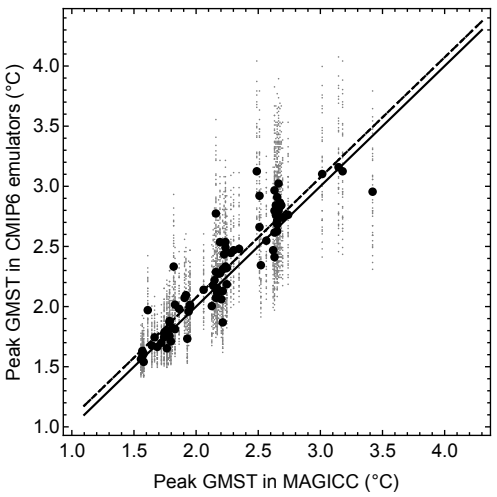

494 FIG. 8. Peak temperatures in MAGICC compared to in CMIP6 ESM emulators. Each small point shows the
495 peak GMST estimated from a ESM emulator and in the MAGICC model for a given emission scenario. The
496 large black points show the average values over each ESM emulator for each scenario. The black dotted line has
497 unit slope and zero intercept and the dashed line is a linear fit to the data.

Figures

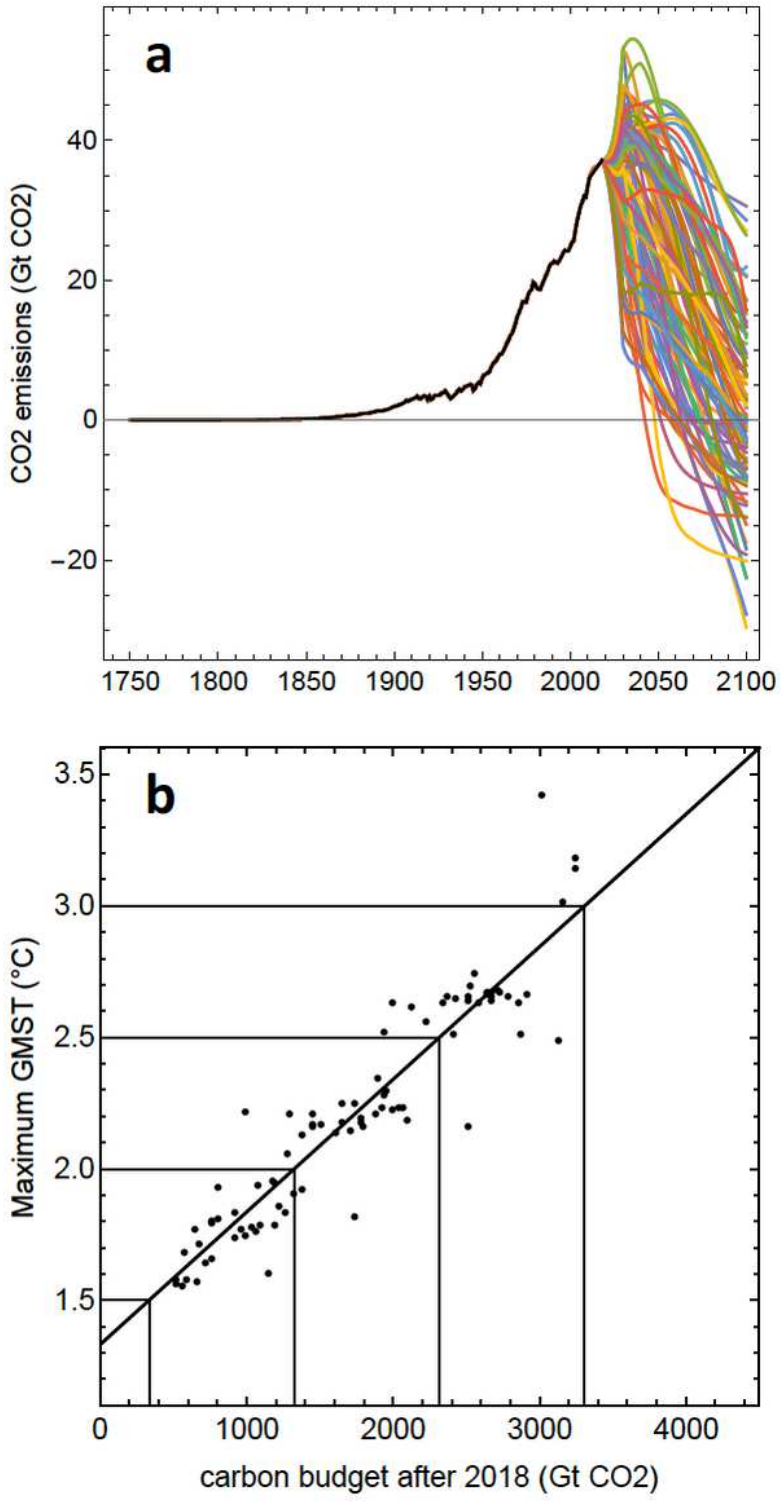

Figure 1

Emission scenarios and RCB estimates from the MAGICC model. (a) The 86 emission scenarios analyzed in this paper. They are collected from the Integrated Assessment Modeling Consortium & International Institute for Applied Systems Analysis (IIASA) (Huppmann et al. 2018) . (b) The plot shows peak GMST

versus cumulative positive emissions after 2018 evaluated by the MAGICC model. The lines explicitly show the RCBs for this particular model, for the GMST targets 1.5, 2, 2.5, and 3°C.

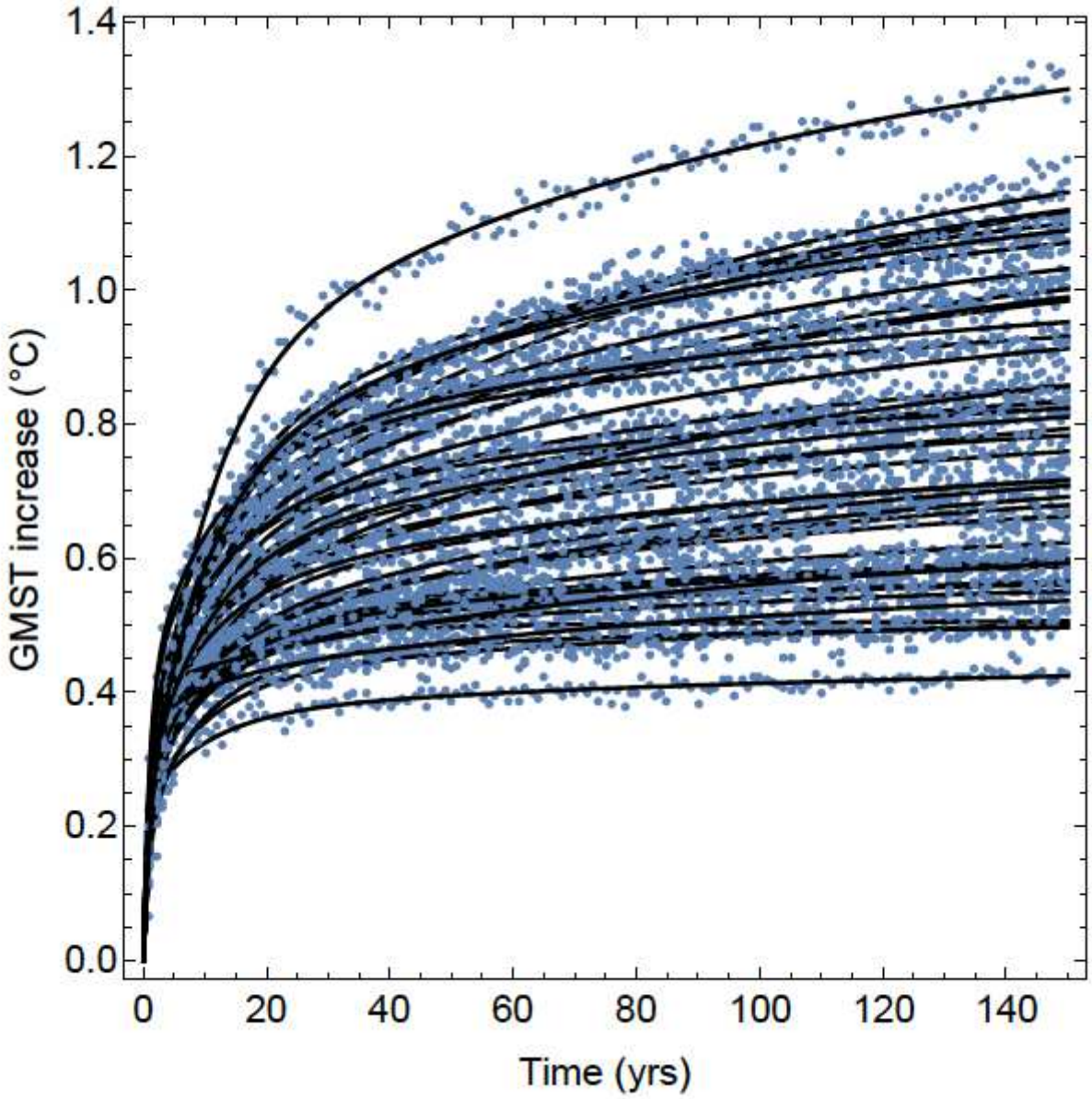

Figure 2

ESM emulators in the CMIP6 ensemble fitted to 4×CO2 runs. The points show the temperature increase over the first 150 yrs after an abrupt quadrupling of CO2 normalized by dividing by the Gregory-estimate of the forcing. The black curves are the fitted temperature responses as described in the Methods section

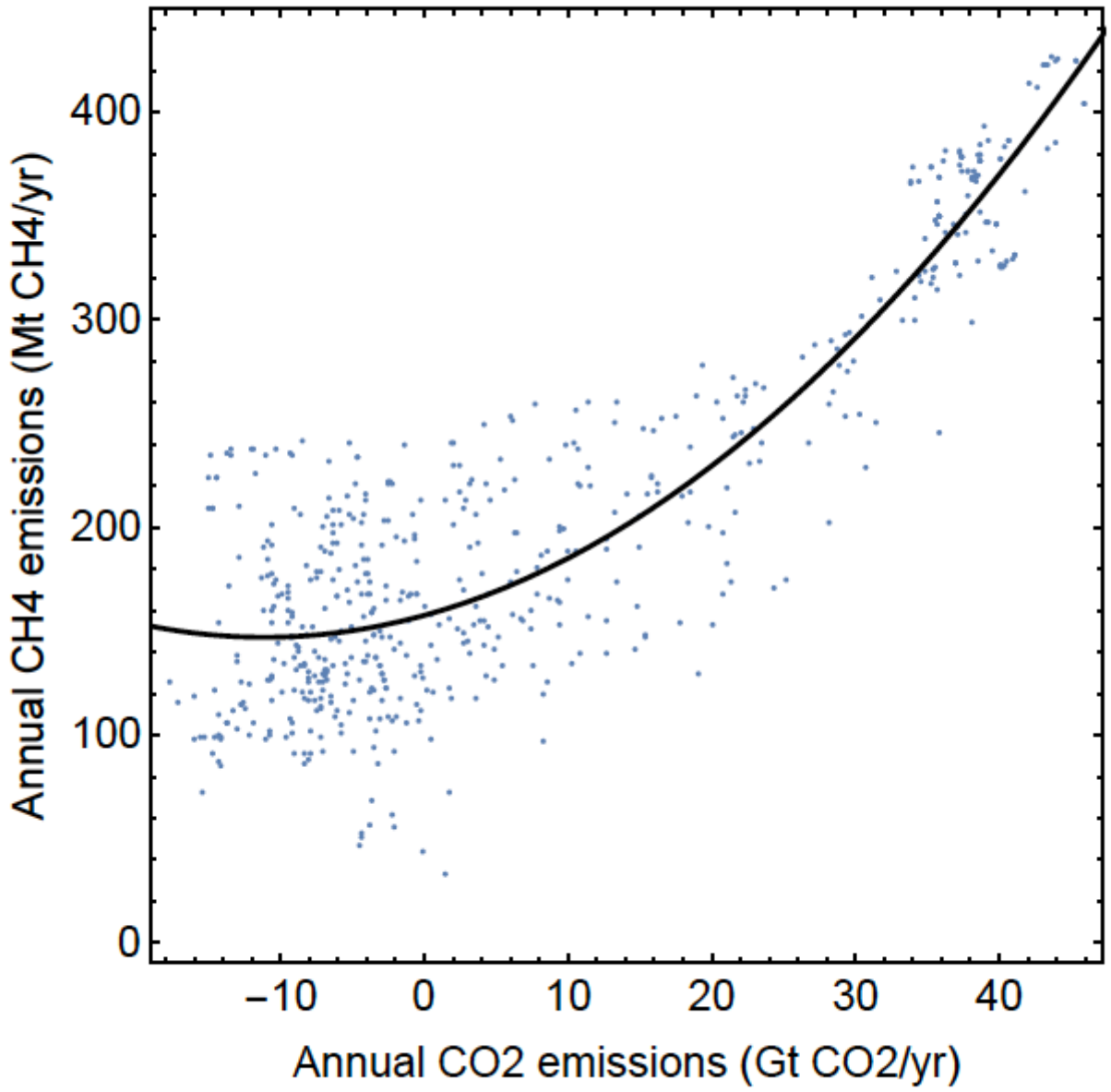

Figure 3

The dependence between CO2 and methane emissions in the scenario database. The points show the annual methane emissions versus the annual CO2 emissions for each emission scenario and each year from 2018 to 2100. The curve show a quadratic fit to the points.

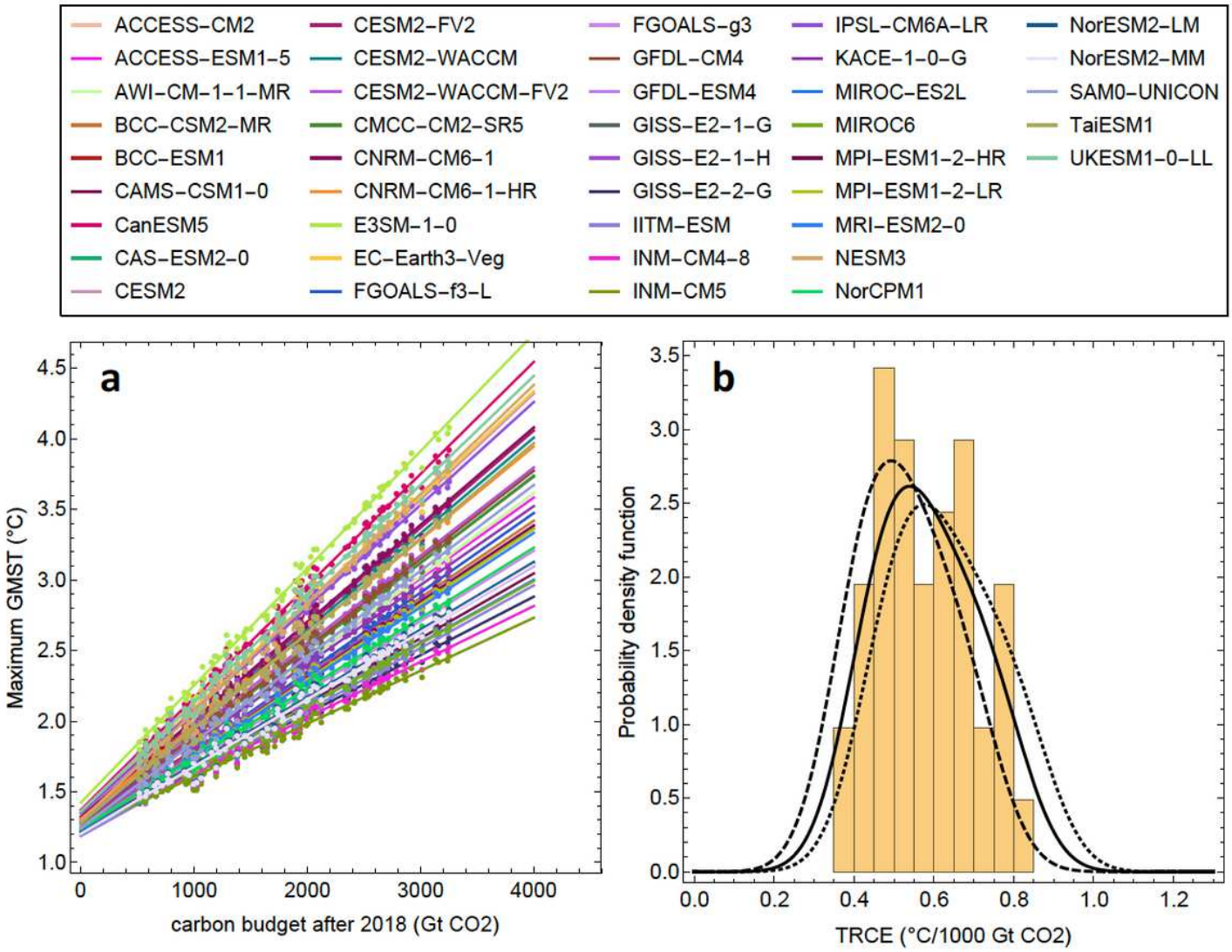

Figure 4

Estimates of TRCE from CMIP6 emulators. (a) Shows the approximately linear relationship between total positive CO2 emissions between 2018 and 2100 and the maximum GMST for 86 emission scenarios and evaluated with emulators of 41 different climate models in the CMIP6 ensemble. Each color represents a climate model and each point an emission scenario. The lines are fitted for each model using linear regression. (b) The histogram shows the distribution of the TCRE obtained from the slopes of the linear fits in Fig. 2a for the 41 different climate model emulators. The solid curve is a smooth kernel estimate of the probability density. The dotted and dashed curves are the estimated probability densities for the TCRE when we use the upper- and lower ranges (model mean plus/minus one standard deviation) of the impulse-response carbon model.)

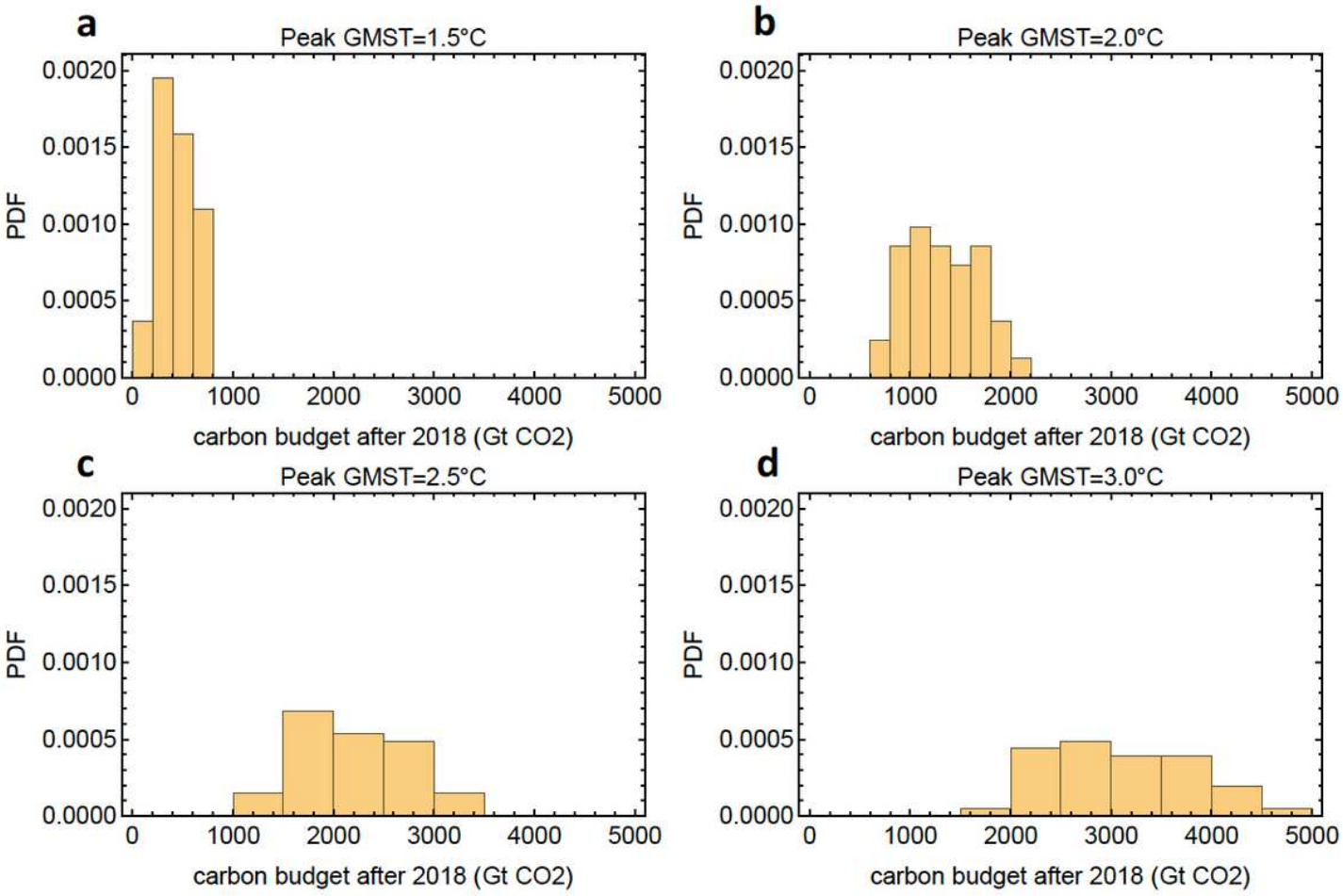

Figure 5

Estimates of RCB for different temperature targets. (a)-(d) show histograms for the 1.5, 2.0, 2.5, and 3.0 °C-targets, respectively.

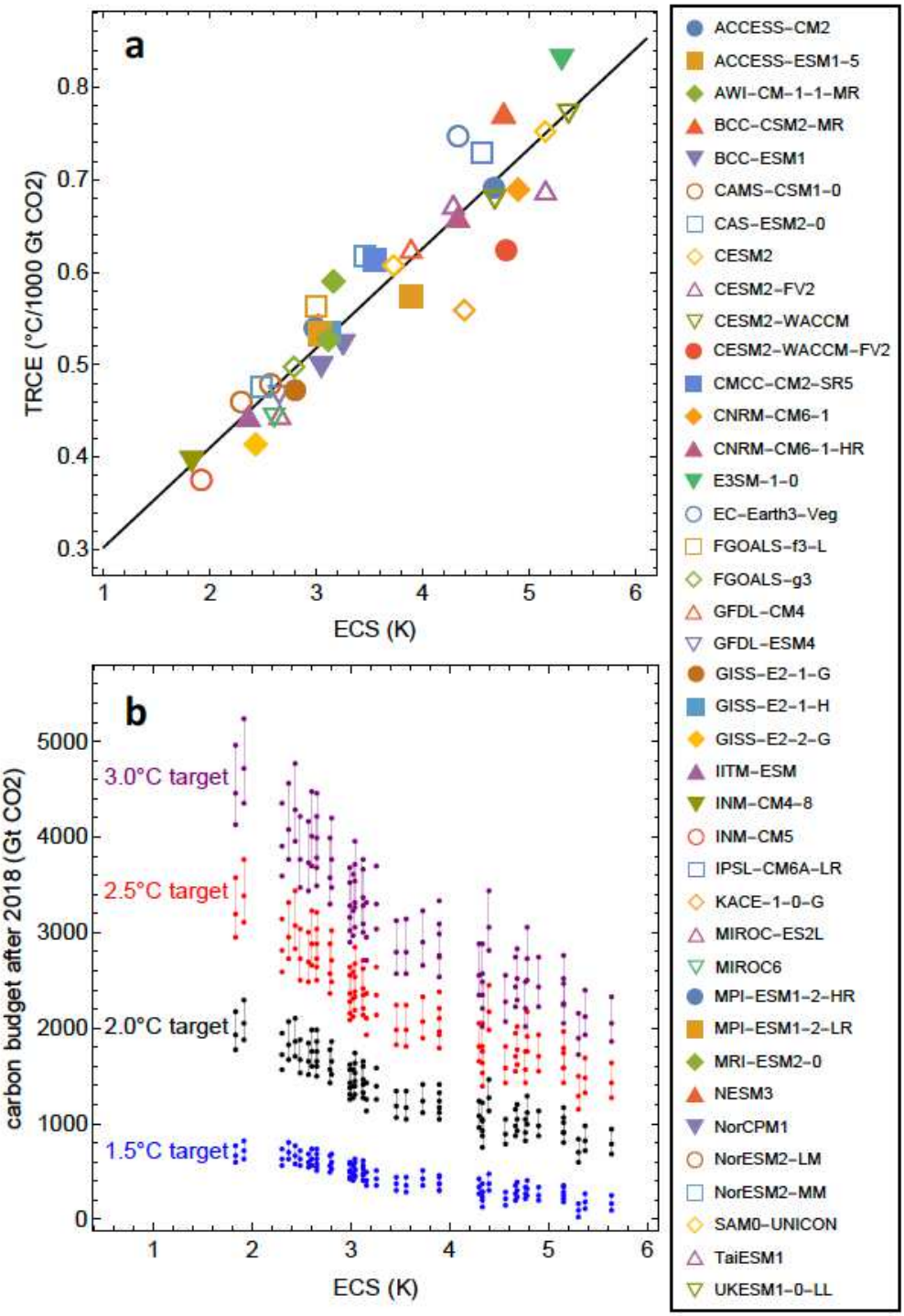

Figure 6

The relationship between RCBs and ECS in the CMIP6 ESM emulators. (a) Shows the approximately linear relationship between the TCRE of the ESM emulators and the ECS estimated from Gregory-plots for 41 models in CMIP6. (b) Shows the RCBs for different maximum GMST targets as against the ECS of the climate model. The points are obtained using the multi-model mean impulse-response carbon model and the upper- and lower ranges (multi-model mean plus/minus one standard deviation).

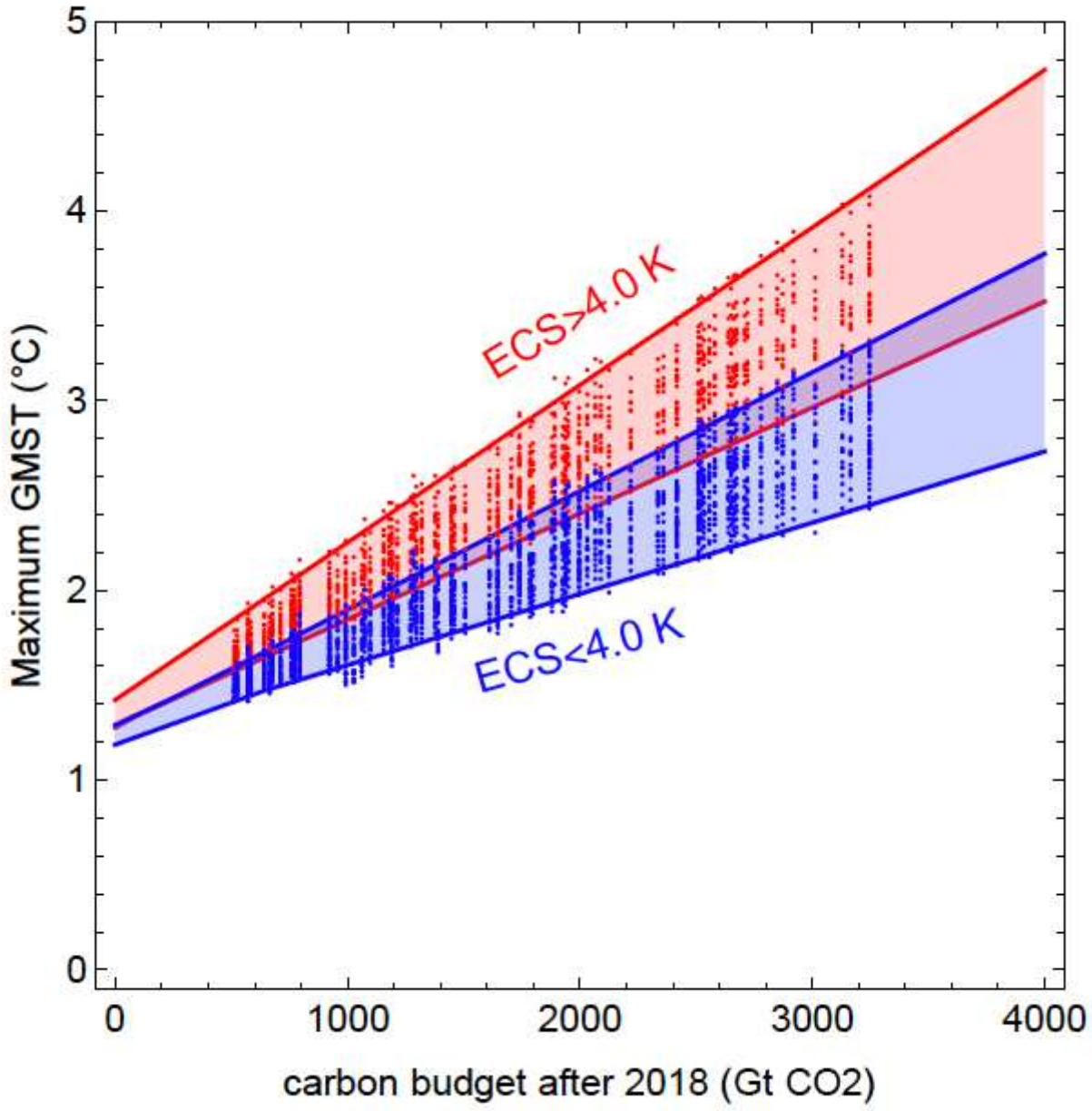

Figure 7

Linear relationships between total positive CO2 emissions and peak GMST for models with high- and low ECS. Shows the same data as in Fig. 4a, but colored so that models with ECS>4.0 K are in red and models with ECS<4.0 K are in blue. The lines show the minimum and maximum TCRE for the two ranges of ECS.

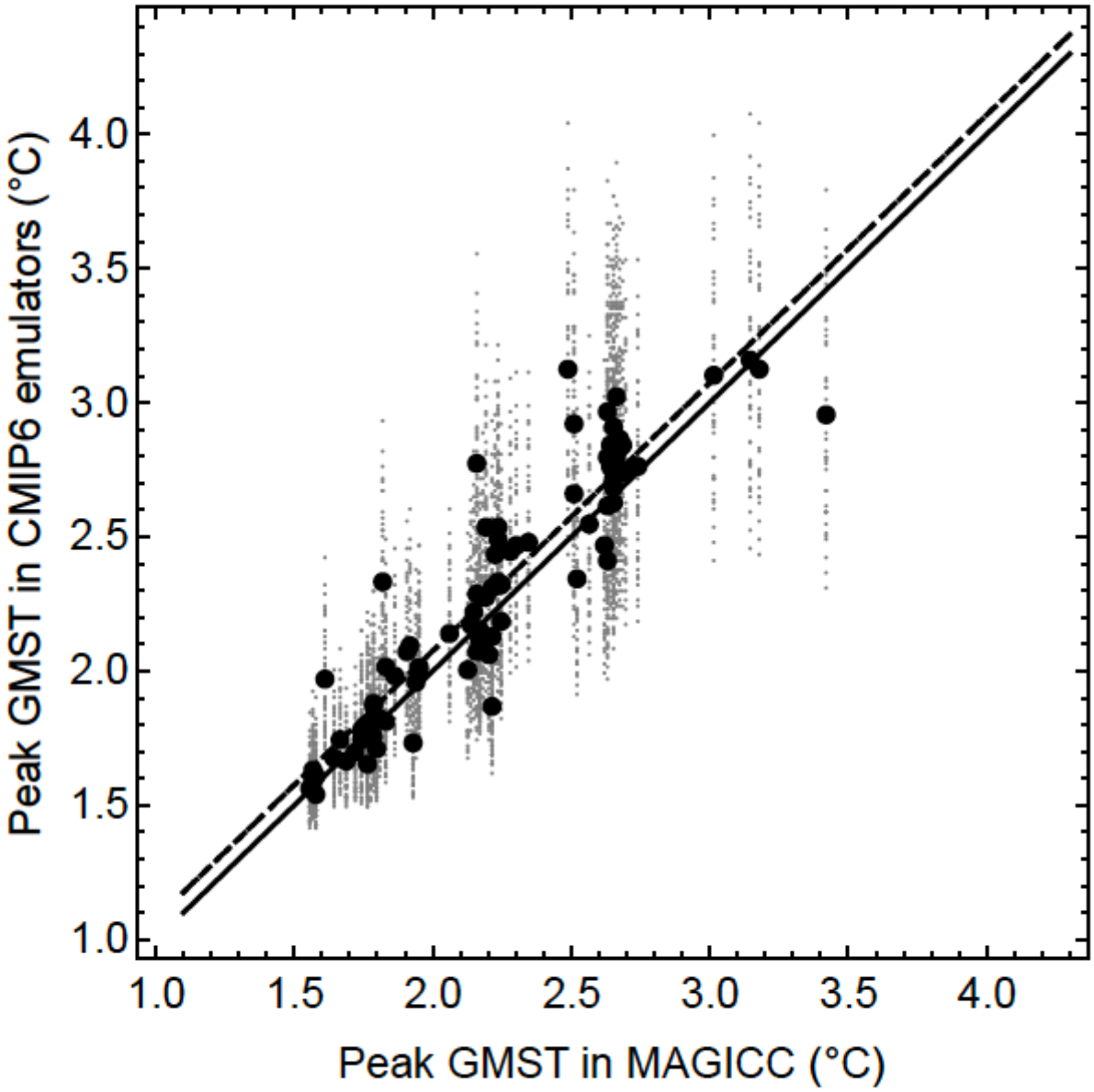

Figure 8

Peak temperatures in MAGICC compared to in CMIP6 ESM emulators. Each small point shows the peak GMST estimated from a ESM emulator and in the MAGICC model for a given emission scenario. The large black points show the average values over each ESM emulator for each scenario. The black dotted line has unit slope and zero intercept and the dashed line is a linear fit to the data.